

# Scalable Quantum-Classical DFT Embedding for NISQ Molecular Simulation

Namrata Manglani  
 AICTE Industry Fellow, C-DAC  
 Pune, India  
 Assistant Professor in Physics  
 Shah and Anchor Kutchhi Engineering College  
 Mumbai, India  
 namrata.manglani@sakec.ac.in

Samrit Kumar Maity  
 C-DAC  
 Pune, India  
 samritm@cdac.in

Ranjit Thapa  
 SRM University-AP  
 Amaravati, India  
 ranjit.t@srmap.edu.in

Sanjay Wandhekar  
 C-DAC  
 Pune, India  
 sanjayw@cdac.in

**Abstract**—Scalable quantum-classical embedding is essential for chemically meaningful simulations on near-term NISQ hardware. Using QDFT, we show systematic correlation energy recovered relative to the DFT baseline, measured against CCSD in a fixed six-orbital active space across molecules from water to naphthalene. By varying embedded electrons from 2 to 8, aromatic systems saturate near 63–64%, while linear molecules like carbon dioxide reach 68%. All systems converge within two embedding iterations under relaxed self-consistency thresholds, highlighting robustness. A (4e,6o) active space recovers 60% correlation using 10 qubits, providing practical NISQ guidelines.

**Index Terms**—DFT embedding, VQE, NISQ, active space, adaptive density damping, aromatic saturation, correlation recovery, quantum chemistry, CASSCF saturation, range-separated DFT

## I. INTRODUCTION

Accurate electronic structure simulations require correlation beyond mean-field DFT, yet exact methods such as full configuration interaction scale factorially with system size. While CCSD and CCSD(T) provide a practical alternative, their computational cost typically limits applications to  $\sim 50$  electrons [1]. Near-term noisy intermediate-scale quantum (NISQ) devices offer the potential to accelerate correlation calculations via the variational quantum eigensolver (VQE) [2], but hardware constraints often restrict the size of feasible active spaces [3].

Quantum embedding on a density functional theory baseline [4] (QDFT) addresses this limitation by partitioning molecules into minimal active spaces—here, six orbitals—within a DFT bath, enabling scalable correlation recovery using quantum solvers implemented in Qiskit Nature. In this work, we demonstrate a production-ready NISQ workflow through two key advances. First, we systematically scale the active space from water to naphthalene, revealing that aromatic systems saturate near 63–64% of correlation recovery relative to the DFT baseline, measured against CCSD as a reference at (6e,6o), while for linear  $\text{CO}_2$  continues to scale to 68% (8e,6o). Second, we implement a robust convergence protocol that achieves SCF self-consistency within two embedding

iterations across molecules of 3–18 atoms using adaptive density damping and smart initialisation of the quantum solver.

Together, these results establish a practical framework for near-term quantum chemistry simulations, balancing computational efficiency with chemical accuracy and paving the way for hardware-ready implementations.

## II. COMPUTATIONAL METHODS

### A. Quantum DFT Embedding Framework

All calculations were performed using a range-separated density functional theory (DFT) embedding formalism following Rossmann et al. [4]. The calculations were carried out using Qiskit Nature version 0.7.2 [5] interfaced with PySCF version 2.6.2 [6]. The embedding workflow was implemented using a custom DFTEmbeddingSolver code provided in Ref. [17], which enables reproducibility with currently supported software versions.

The embedding bath was treated using a range-separated local density approximation (LDA) with the Vosko–Wilk–Nusair (VWN) correlation functional. The 6-31G\* basis set was used consistently for the active region, embedding bath, and reference calculations.

Relative to the original Qiskit AquaChemistry prototype [16], the present implementation differs only in numerical stabilization choices: (i) Hartree–Fock initialization of the VQE solver was employed, with variational parameters initialized using a small Gaussian perturbation ( $\sigma = 10^{-3}$ ) to break parameter symmetries and improve optimizer stability. While zero-valued initial parameters were sufficient for convergence in small molecular systems, perturbed initializations were empirically observed to yield more reliable convergence for larger molecules, even when the same active space was retained. (ii) adaptive density damping in the embedding self-consistency cycle,,  $\alpha_i = \max(0.05, 0.2/\sqrt{i})$ , replacing fixed mixing schemes, and (iii) a relaxed but justified embedding convergence threshold of  $10^{-7} \text{ Ha}$ . Convergence thresholds of this magnitude have been shown to yield stable and reliable energies in large-scale self-consistent electronic structure methods [7], [8].

For all molecular systems studied (3–18 atoms), embedding self-consistency was achieved within two embedding iterations.

### B. Range-Separation Parameter Optimization

The range-separation parameter  $\mu$  was optimized individually for each molecular system by minimizing the fully converged quantum DFT embedding energy. For all systems,  $\mu$  was scanned from 0.5 to 10 in increments of 0.25, covering the range from near the pure DFT limit ( $\mu \rightarrow 0$ ) toward the Hartree–Fock limit ( $\mu \rightarrow \infty$ ).

At each  $\mu$ , the embedding equations were iterated to full self-consistency using identical active-space definitions, quantum solvers, and convergence thresholds. Only fully converged embedding solutions were used to evaluate the total embedding energy  $E_{\text{QDFT}}$ . The optimal  $\mu$  was then chosen as the value that yielded the lowest  $E_{\text{QDFT}}$ , and this  $\mu_{\text{opt}}$  was held fixed for all subsequent calculations on the corresponding molecular system.

### C. Active Space and Quantum Solver Details

All embedded quantum calculations employed a fixed active space of six spatial orbitals, while the number of active electrons was systematically increased as (2e,6o), (4e,6o), (6e,6o), and (8e,6o). This protocol enables controlled analysis of correlation recovery and active-space saturation effects across chemically distinct systems.

Second-quantized molecular Hamiltonians were mapped to qubit operators using parity mapping [10] combined with symmetry-based qubit tapering [9] to reduce the required qubit count. The UCCSD ansatz was initialized from a Hartree–Fock (HF) reference state and implemented using a single Trotter step. Variational parameters were initialized from a seeded Gaussian distribution with standard deviation  $\sigma = 0.001$ , ensuring reproducibility and keeping the ansatz close to the HF reference, which improves local curvature estimation and stabilizes convergence of the L-BFGS-B optimizer. VQE optimization was performed using L-BFGS-B [11] with a maximum of 50 iterations and an energy convergence tolerance of  $10^{-6}$ . A callback was used to record energy evaluations during optimization, and all expectation values were computed using an exact (noiseless) quantum estimator, isolating embedding and algorithmic performance from hardware noise effects.

### D. Molecular Systems and Reference Data

The molecular test set comprises Water ( $\text{H}_2\text{O}$ ), Carbon dioxide ( $\text{CO}_2$ ), Benzene ( $\text{C}_6\text{H}_6$ ), Pyridine ( $\text{C}_5\text{H}_5\text{N}$ ), and Naphthalene ( $\text{C}_{10}\text{H}_8$ ) as shown in Figure 1, the latter representing the largest system studied in a quantum DFT embedding context to date. All geometries correspond to equilibrium structures obtained from the NIST Computational Chemistry Comparison and Benchmark Database (CCCBDB) at the B3LYP/6-31G\* level [12].

Reference correlation energies were obtained from coupled-cluster singles and doubles (CCSD) calculations performed in PySCF, using identical geometries and basis sets as employed in the embedding calculations.

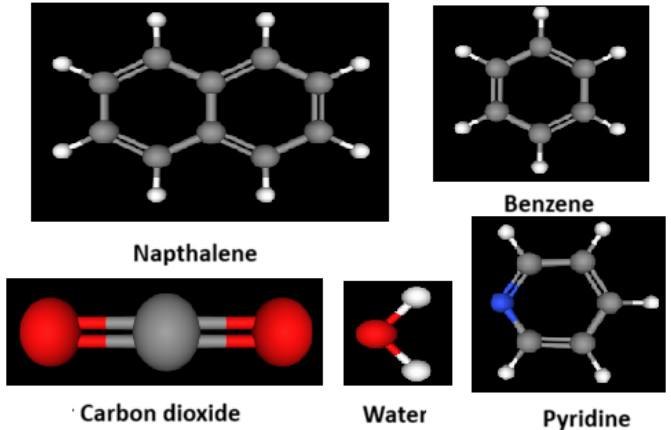


Fig. 1. Representation of molecular structure from MolView

## III. RESULTS AND DISCUSSION

### A. Baseline Energies

Table I reports total energies obtained at the Hartree–Fock (HF), density functional theory (DFT), quantum DFT embedding with a VQE active-space solver (QDFT), and CCSD levels for all systems considered, using a consistent 6-31G\* basis and equilibrium geometries.

Across all molecules, QDFT systematically improves upon both HF and DFT energies and approaches the CCSD reference. This trend is observed consistently for small polar systems ( $\text{H}_2\text{O}$ ), linear molecules ( $\text{CO}_2$ ), and conjugated aromatic systems, demonstrating the robustness of the embedding protocol across chemically diverse regimes.

TABLE I  
BASELINE TOTAL ENERGIES (HA) AND SYSTEM SIZES USING  
BEST-PERFORMING ACTIVE SPACES (CAS).

Molecule	Atoms	HF	DFT	QDFT (e,o)	CCSD
Water	3	-76.008	-75.841	-76.067 (6,6)	-76.205
Carbon dioxide	3	-187.630	-187.174	-187.805 (8,6)	-188.102
Benzene	12	-230.701	-230.074	-230.990 (6,6)	-231.502
Pyridine	11	-246.693	-246.043	-246.979 (6,6)	-247.519
Naphthalene	18	-383.353	-382.319	-383.818 (6,6)	-384.673

### B. Correlation Recovery and Active-Space Scaling

The recovery fraction

$$R = 100 \times \frac{E_{\text{QDFT}} - E_{\text{DFT}}}{E_{\text{CCSD}} - E_{\text{DFT}}} \quad (1)$$

quantifies the fraction of correlation energy recovered by QDFT. Here,  $E_{\text{DFT}}$  is the total energy from a Restricted Kohn Sham(RKS) PySCF calculation using the 6-31G\* basis set and the LDA (VWN) functional,  $E_{\text{QDFT}}$  is the corresponding energy obtained with quantum embedding applied to the same DFT description, and  $E_{\text{CCSD}}$  is the coupled-cluster singles and doubles reference energy. A value of  $R = 0\%$  corresponds to plain DFT, while  $R = 100\%$  indicates full recovery of the CCSD correlation energy.

Table II summarizes the maximum correlation recovery obtained for fixed six-orbital active spaces while systematically increasing the number of correlated electrons. All systems exceed 60% recovery at modest active-space sizes (Results for water and pyridine can be compared with [4]), with  $\text{CO}_2$  reaching a maximum of 68.0% at (8e,6o). Aromatic systems exhibit a clear plateau, saturating near 63–64% recovery at (6e,6o).

TABLE II  
CCSD CORRELATION RECOVERY (%) AS A FUNCTION OF ACTIVE-SPACE SIZE FOR FIXED SIX-ORBITAL SUBSPACES.

Molecule	$\mu_{\text{opt}}$	(2e,6o)	(4e,6o)	(6e,6o)	(8e,6o)
Water	7.25	61.7	60.1	<b>62.1</b>	61.4
Carbon dioxide	6.75	63.6	66.3	66.8	<b>68.0</b>
Benzene	5.00	62.6	<b>64.1</b>	64.1	64.1
Pyridine	5.25	62.0	<b>63.4</b>	63.4	63.4
Naphthalene	5.00	62.2	62.9	<b>63.7</b>	63.0

### C. Active-Space Convergence Trends

Figure 2 illustrates correlation recovery as a function of active-space electron count for all systems. A 60% recovery threshold (dashed line) is exceeded in all cases once four or more electrons are correlated, demonstrating efficient convergence within small active spaces.

$\text{CO}_2$  exhibits the most favorable scaling behavior, continuing to gain correlation energy up to (8e,6o), whereas aromatic systems plateau at approximately 63–64% recovery. This behavior is consistent with the rapid saturation of  $\pi$ -correlation in cyclic conjugated systems reported in multireference studies [13], [14] and in quantum embedding contexts [4], [15].

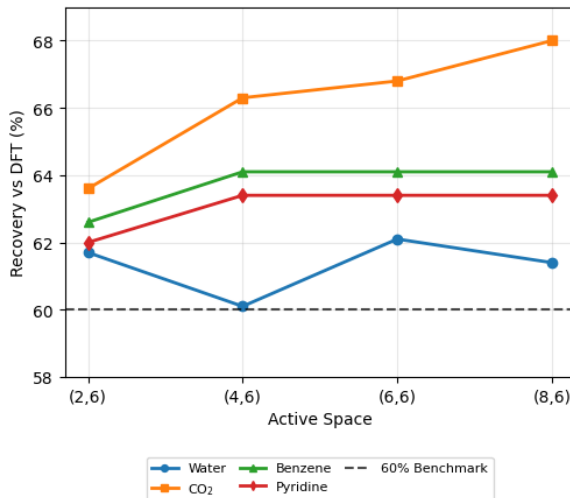


Fig. 2. Correlation recovery versus active-space size. The dashed line indicates 60% recovery. Linear  $\text{CO}_2$  continues to scale, while aromatic systems saturate at modest active spaces.

### D. Discussion

The central result of this work is that QDFT provides systematic and size-consistent improvements over classical DFT while maintaining a fixed quantum computational cost as molecular size increases. Across systems ranging from 3 to 18 atoms, a substantial fraction of the CCSD correlation energy is consistently recovered relative to the DFT baseline, demonstrating that strong correlation can be efficiently localized within a compact quantum active space.

Fixed six-orbital active spaces recover over 60% of CCSD correlation energy across chemically diverse molecules, corresponding to approximately 10 qubits after symmetry tapering. This establishes a practical operating regime for NISQ hardware and highlights a key advantage of embedding methods: quantum resource requirements remain decoupled from overall system size [15].

Correlation recovery trends reflect molecular structure. Aromatic systems exhibit early saturation near 63–64%, consistent with rapid convergence of dominant  $\pi$ -electron correlations once essential near-degeneracies are included. In contrast, the linear molecule  $\text{CO}_2$  continues to benefit from correlating additional electrons, reaching up to 68% recovery at (8e,6o).

Numerically, the embedding procedure converges robustly across all systems, typically within two iterations using a relaxed SCF threshold of  $10^{-7}$  Ha. This stability is enabled by small random VQE initialization and adaptive density damping, supporting the feasibility of QDFT embedding for NISQ-era simulations.

### IV. CONCLUSIONS

Range-separated DFT embedding with a quantum active-space solver recovers 60–68% of CCSD correlation energy using compact active spaces (up to 8 electrons in 6 orbitals), demonstrated across  $\text{H}_2\text{O}$ ,  $\text{CO}_2$ , benzene, pyridine, and naphthalene (6-31G\*, LDA) [Tables I–II].

Key advances for hybrid quantum chemistry include: (1) Fixed active spaces decouple quantum cost from molecular size up to 18 atoms, (2) Small random VQE initialization and adaptive density damping ensure rapid convergence in two iterations

Correlation trends reflect chemical structure: linear  $\text{CO}_2$  continues scaling to 68% at (8e,6o), while aromatic systems saturate efficiently near 64% at (6e,6o) [Fig. 2], consistent with rapid  $\pi$ -electron correlation convergence in cyclic systems.

Future directions include systematic evaluation of higher-level functionals in the DFT bath, execution on quantum hardware with noise-mitigation strategies compatible with compact active spaces, and extension to strongly multireference or excited-state systems.

Overall, this study establishes quantum DFT embedding as a scalable and chemically interpretable approach, bridging near-term quantum simulations and realistic molecular applications.

### ACKNOWLEDGMENT

The author(s) gratefully acknowledge the support of the AICTE Industry Fellowship Scheme for funding and facil-

itating this research. The guidance and resources provided under this program have been invaluable in carrying out this work. The author(s) also thank the Centre for Development of Advanced Computing (C-DAC) and the National Supercomputing Mission (NSM) for providing computational resources and technical support, which significantly contributed to the completion of this research.

## REFERENCES

- [1] R. J. Bartlett and M. Musial, “Coupled-cluster theory in quantum chemistry,” *Rev. Mod. Phys.* **79**, 291 (2007), <https://doi.org/10.1103/RevModPhys.79.291>.
- [2] A. Peruzzo, J. McClean, P. Shadbolt, M.-H. Yung, X.-Q. Zhou, P. J. Love, A. Aspuru-Guzik, and J. L. O’Brien, “A variational eigenvalue solver on a photonic quantum processor,” *Nat. Commun.* **5**, 4213 (2014), <https://doi.org/10.1038/ncomms5213>.
- [3] S. McArdle, T. Endo, A. Aspuru-Guzik, S. C. Benjamin, and G. H. Low, “Quantum computational chemistry,” *Rev. Mod. Phys.* **92**, 015003 (2020), <https://doi.org/10.1103/RevModPhys.92.015003>.
- [4] M. Rossmanek, P. K. Barkoutsos, P. J. Ollitrault, and I. Tavernelli, “Quantum HF/DFT-embedding algorithms for electronic structure calculations: Scaling up to complex molecular systems,” *arXiv:2009.01872 [quant-ph]* (2020), *J. Chem. Phys.* **154**, 114105 (2021), <https://arxiv.org/abs/2009.01872>, <https://doi.org/10.1063/5.0029536>.
- [5] Qiskit Nature Development Team, “Qiskit Nature 0.7 Documentation,” <https://qiskit-community.github.io/qiskit-nature> (2025).
- [6] Q. Sun, T. C. Berkelbach, N. S. Blunt, G. H. Booth, S. Guo, Z. Li, J. Liu, J. D. McClain, E. R. Sayfutyar, S. Sharma, S. Wouters, and G. K.-L. Chan, “PySCF: The Python-based simulations of chemistry framework,” *WIREs Comput. Mol. Sci.* **8**, e1340 (2018), <https://doi.org/10.1002/wcms.1340>.
- [7] F. Pes, M. Repisky and R. Bast, ‘A Quasi Time-Reversible Scheme Based on Density Matrix Purification,’ *J. Chem. Theory Comput.* **19**, 6789 (2023). <https://pmc.ncbi.nlm.nih.gov/articles/PMC10626629/>
- [8] A. Foerster, F. Wilhelmus and P. Schwerdtfeger, ‘Low-Order Scaling Quasiparticle Self-Consistent GW,’ *J. Chem. Theory Comput.* **17**, 5502 (2021). <https://pmc.ncbi.nlm.nih.gov/articles/PMC8446457/> ; remove extra keep only cited ones
- [9] S. Bravyi, J. M. Gambetta, A. Mezzacapo, and K. Temme, “Tapering off qubits to simulate fermionic Hamiltonians,” *arXiv preprint arXiv:1701.08213*, 2017. [Online]. Available: <https://arxiv.org/abs/1701.08213>
- [10] J. T. Seeley, M. J. Richard, and P. J. Love, “The Bravyi-Kitaev transformation for quantum computation of electronic structure,” *J. Chem. Phys.*, vol. 137, no. 22, p. 224109, 2012. doi:10.1063/1.4768229.
- [11] R. H. Byrd, P. Lu and J. Nocedal, “A Limited Memory Algorithm for Bound Constrained Optimization,” *SIAM J. Sci. Stat. Comput.* **16**, 1190 (1995). <https://doi.org/10.1137/0916069>
- [12] NIST Computational Chemistry Comparison and Benchmark Database, NIST Standard Reference Database Number 101, Release 22, May 2022, Editor: Russell D. Johnson III, <https://cccbdb.nist.gov/>.
- [13] B. O. Roos and P. A. Malmqvist, “How to select active space for multiconfigurational quantum chemistry?” *Int. J. Quantum Chem.* **111**, 3329 (2011).
- [14] P. Celani and H.-J. Werner, “Multiconfigurational self-consistent field theory. Basis set and active space convergence,” *J. Chem. Phys.* **102**, 10241 (1995).
- [15] S. Battaglia, F. G. B. N. de Sousa, and M. Reiher, “A general framework for active space embedding methods: applications in quantum computing,” *arXiv:2404.18737* (2024).
- [16] Max Rossmanek, qiskit-nature-pyscf-dft-embedding GitHub repository, 2022 [<https://github.com/mrossinek/qiskit-nature-pyscf-dft-embedding>]
- [17] N. Mangani, ‘DFT Quantum Embedding,’ GitHub repository, [<https://github.com/NamrataaKkommineni/DFT-Quantum-Embedding>] (2026).